

Manuscript Number: MEP-D-15-00453

Title: Gaussian process prediction of the stress-free configuration of  
pre-deformed soft tissues: Application to the human cornea

Article Type: Paper

Section/Category: Regular Issue Paper

Keywords: biomechanics, prediction, finite-element, Gaussian Process,  
Cornea, stress-free

Corresponding Author: Dr. Philippe Buechler, PhD

Corresponding Author's Institution: University of Bern

First Author: Elena Businaro

Order of Authors: Elena Businaro; Harald Studer; Bojan Pajic; Philippe  
Buechler, PhD

Abstract: Image-based modeling is a popular approach to perform patient-specific biomechanical simulations. One constraint of this technique is that the shape of soft tissues acquired in-vivo is deformed by the physiological loads. Accurate simulations require determining the existing stress in the tissues or their stress-free configurations. This process is time consuming, which is a limitation to the dissemination of numerical planning solutions to clinical practice. In this study, we propose a method to determine the stress-free configuration of soft tissues using a Gaussian Process (GP) regression. The prediction relies on a database of pre-calculated results to enable real time predictions. The application of this technique to the human cornea showed a level of accuracy five to ten times higher than the accuracy of the topographic device used to obtain the patients' anatomy. In this context, we believe that GP models are suitable for predicting the stress free configuration of the cornea and can be used in planning tools based on patient-specific finite element simulations. Due to the high level of accuracy required in ophthalmology, this approach is likely to be appropriate for other applications requiring the definition of the relaxed shape of soft tissues.

## \*Highlights (for review)

- Gaussian Process (GP) regression was proposed to obtain the stress-free configuration of soft tissues measured under physiological loads
- Application on the human cornea was based on more than 1000 datasets
- Determination of the stress-free configuration is instantaneous
- The stress-free configuration was at least five 5 times more accurate than the clinical requirements

# Gaussian process prediction of the stress-free configuration of pre-deformed soft tissues: Application to the human cornea

---

Elena Businaro<sup>1,2</sup>, Harald Studer<sup>2</sup>, Bojan Pajic<sup>3,4,5,6</sup> & Philippe Büchler<sup>1</sup>

<sup>1</sup>Institute for Surgical Technology & Biomechanics, University of Bern, Switzerland

<sup>2</sup>Integrated Scientific Services AG, Biel, Switzerland

<sup>3</sup>Swiss Eye Research Foundation, Eye Clinic ORASIS, Reinach AG, Switzerland

<sup>4</sup>Division of Ophthalmology, Department of Clinical Neurosciences, University Hospitals of  
Geneva, Switzerland

<sup>5</sup>University of Novi Sad, Faculty of Sciences, Faculty of Physics, Novi Sad, Serbia

<sup>6</sup>Medical faculty, Military Medical Academy, University of Defense Belgrade, Serbia

20 Address for correspondence:

21 Philippe Büchler

22 Institute for Surgical Technology & Biomechanics

23 University of Bern

24 Stauffacherstrasse 78

25 3014 Bern, Switzerland

26 Phone: +41 31 631 5947

27 Email: [philippe.buechler@istb.unibe.ch](mailto:philippe.buechler@istb.unibe.ch)

28

30

**Abstract**

31 Image-based modeling is a popular approach to perform patient-specific biomechanical  
32 simulations. One constraint of this technique is that the shape of soft tissues acquired in-vivo  
33 is deformed by the physiological loads. Accurate simulations require determining the existing  
34 stress in the tissues or their stress-free configurations. This process is time consuming,  
35 which is a limitation to the dissemination of numerical planning solutions to clinical practice.  
36 In this study, we propose a method to determine the stress-free configuration of soft tissues  
37 using a Gaussian Process (GP) regression. The prediction relies on a database of pre-  
38 calculated results to enable real time predictions. The application of this technique to the  
39 human cornea showed a level of accuracy five to ten times higher than the accuracy of the  
40 topographic device used to obtain the patients' anatomy. In this context, we believe that GP  
41 models are suitable for predicting the stress free configuration of the cornea and can be used  
42 in planning tools based on patient-specific finite element simulations. Due to the high level of  
43 accuracy required in ophthalmology, this approach is likely to be appropriate for other  
44 applications requiring the definition of the relaxed shape of soft tissues.

45

## 1 Introduction

The recent progress in medical image analysis and numerical simulation tools enabled the development of patient-specific planning solutions based on biomechanical simulations. The anatomical information for each patient is derived from medical imaging and finite element simulations are used to evaluate the outcome of specific surgical interventions. Additionally, such simulation platforms allow further understanding of the disease, its progression and on the efficacy of available treatments and procedures.

One of the problems with this approach is that the medical images acquired in-vivo describe the tissue in its physiological situation, which is frequently under stress. This is typically the case for soft tissue such as ligaments, arteries or the human eye. However, the level of initial strain in the tissue cannot be directly measured on the patient, therefore the biomechanical models are considering an initially unloaded “stress-free” configuration[1]. Several methods were proposed to pre-stress the measured ‘initial’ geometry[1-4]. Among these methods, some researchers proposed an inverse elastostatic approach centered on the reverse application of in-vivo conditions to explicitly estimate the stress-free configuration, hence one non-linear simulation step is required to update the deformation gradient tensor [5–7]. Others adopted a modified updated Lagrangian formulation [1,2,8], to estimate the stress in the tissue using a forward calculation, where the procedure continuously updates the deformation tensor during the simulation of the in-vivo state. Although these methods provided accurate results, they require complex implementations, and – especially when the tissue is considered incompressible – a thorough knowledge of continuum mechanics as well as the solution of a non-linear problem. By contrast, an easier approach has been proposed by Pandolfi [9], where a simple analytic calculation is combined with finite element analysis to obtain the stress-free configuration of the tissue. High accuracy can be achieved with this approach, but the solution requires the iterative solution of a finite element problem, which is time consuming[2,11,24].

Calculation time represents an important issue for the acceptability of the planning tool in clinical routine. Therefore, the stress-free configuration of the tissues should be obtained as efficiently as possible. For this reason, the aim of this study was to evaluate prediction of the relaxed shape of the tissue with a stochastic approach. The Gaussian process (GP) is one of the most widely used stochastic and non-parametric processes for modeling dependent data observed over space or time. It has been used for several biomechanical applications to predict human gait kinematics [15], abdominal aortic aneurysms [16] or for the estimation of swimming velocity [17]. Our hypothesis was that this method could also be suitable to estimate the patient-specific stress-free configuration starting from clinical images. In this work, the parameters describing the shape of the tissue were modeled as a Gaussian process, which was used to predict the stress-free configuration without any further finite-element analysis. The method has been applied in ophthalmology for the prediction of the relaxed shape of the cornea that will be used in a planning solution for refractive surgeries.

## **2 Material & Methods**

In order to compute the stress free configuration of the cornea using a Gaussian Process approach, several steps were necessary. First, the corneal geometrical information was acquired with a topography device (Section 2.1); the geometrical information thus obtained was used to deform a spherical cornea template to create patient-specific finite element meshes (Section 2.2). Patient specific models were then pre-stressed with an iterative approach (Section 2.3) and the resulting stressed corneas were divided into training and test data (Section 2.4.1). The training data was used to build the Gaussian process model (Section 2.4.2) and the test data was used to assess the quality of the prediction obtained with the fitted Gaussian process model (Section 2.4.3).

### **2.1 Patient Data**

The shape of 1738 patients corneas were acquired with a Pentacam HR Scheimpflug camera. This topography device allows an accurate measurement of the anterior and

98 posterior surface of the cornea (accuracy of a few microns) and to export the geometric  
 99 measurements as Zernike[18] polynomials. The Zernike coefficients  $W(r, \theta)$  describe the  
 100 elevation data of both the anterior and the posterior corneal surfaces. This decomposition is  
 101 frequently used to describe the shape of the corneal surface, because the Zernike  
 102 polynomials  $Z_n^m$  represent an orthonormal basis where each polynomial function describes a  
 103 distinct optical property of the refractive surface (i.e. defocus, astigmatism, coma, trefoil,  
 104 quadrafoil). Therefore, any points on the corneal surface can be defined in a polar coordinate  
 105 system  $r, \theta$  as:

$$W(r, \theta) = \sum_{n=0}^k \sum_{m=-n}^n W_n^m Z_n^m(r, \theta)$$

106 where  $W_n^m$  are the Zernike coefficients defining the weights,  $n$  and  $m$  are respectively the  
 107 order and phase of the polynomial. Zernike polynomials up to order  $k \leq 6$  have been  
 108 considered in this study.

## 109 2.2 Finite element model

110 Patient-specific models of the cornea were obtained by morphing a template finite element  
 111 mesh to the topographic measurements. The three-dimensional template mesh included both  
 112 the cornea and sclera (Figure 1), which were meshed with about 40000 linear hexahedral  
 113 elements [20]. A no-displacement boundary condition has been applied to the nodes located  
 114 on the cut-section through the sclera. A normal intraocular pressure of 15 mmHg has been  
 115 applied on the internal surface of the mesh.

116 A mechanical model previously published and validated has been used to describe the  
 117 mechanical behavior of the tissue [19,20]. Briefly, the strain energy function of the constitutive  
 118 material model is given below:

$$\Psi = U + \bar{\Psi}_m + \frac{1}{\pi} \int \Phi(\theta) \cdot (\bar{\Psi}_{f1} + \bar{\Psi}_{f2}) d\theta$$



where  $U$  describes a penalty function to ensure incompressibility of the material,  $\bar{\Psi}_m$  is a neo-Hookean material representing the tissue matrix,  $\bar{\Psi}_{f1}$  and  $\bar{\Psi}_{f2}$  are modified Ogden materials [21] modeling the main collagen fibers and the collagen cross-linking, respectively. The probability distribution function  $\Phi$  defines a realistic fiber distribution [22] by assigning weights to each fiber direction. Material constants were determined using three sets of experimental data obtained on button inflation tests [23] and strip extensimetry [14].

### 2.3 Iterative Pre-Stressing Process

The in-vivo corneal shape measured by the Pentacam device was stressed by the physiological intraocular pressure. An iterative approach was applied to progressively move the nodes of the patient-specific finite element mesh toward their stress-free shape. In this study the iterative approach, proposed by Elsheikh et al. [24] and Pandolfi et al. [9], was used.

Assuming the coordinates of the patient-specific model ( $X_0$ ) as the target of the iterative process,  $x_i$  describes the corneal geometry after each iteration  $i$  resulting from the nodal displacement induced by the intraocular pressure (IOP). The computed nodal displacements  $u_i$  are then used to estimate the stress-free form  $X_i$  and the error  $e_i$ :

$$e_i = x_i - X_0 = (X_i + u_i) - X_0$$

$$X_{i+1} = X_0 - u_i$$

The root mean square distance was used to monitor the convergence of the iterative process to the stress-free form. The iterative process was stopped when this error dropped below  $10^{-4}$   $\mu\text{m}$ , which usually requires about 10 iterations.

### 2.4 Gaussian Process

A Gaussian process was defined to predict the stress-free configuration of the cornea. The model parameters were fitted to generate a functional mapping between the shape of the cornea measured experimentally and the corresponding stress-free configuration. In this

study, the Matlab implementation of Gaussian Process for Machine Learning proposed by Rasmussen[25] has been used.

#### 2.4.1 Training and Test Datasets

This dataset consists of training input vectors  $x_s$ , containing the Zernike coefficients describing the shape of each patient's cornea under stress, as well as training output vectors  $y_s$ , containing the Zernike coefficients describing the stress-free shape of these corneas. The parameters of the output matrix  $y_s$  were obtained with the pre-stressing technique described previously.

The training dataset represents the pool of data that was used to determine the Gaussian Process. To evaluate the effect of the size of the training data on the predictions, several GP models were fitted on gradually increasing number of training data. Four GP models have been fitted to datasets containing 250, 500, 750 and 1663 corneas. In this evaluation the training dataset included a mix of healthy and pathological corneas, while the test dataset consisted of 75 healthy corneas.

Further GP models were built to verify the effect of discriminating healthy from pathological corneas within the training dataset. For this evaluation, we used two training datasets, each containing 700 corneas from healthy and pathological patients, respectively. Separate datasets containing respectively 75 pathological and 73 healthy corneas were used to evaluate the quality of the predictions.

#### 2.4.2 Design of Gaussian process model

A GP can be considered as a collection of random variables indexed by a continuous variable:  $f(x)$ . Suppose we define a particular finite subset of these random variables  $f(x) = \{f_1, f_2, \dots, f_N\}$ , with corresponding inputs  $x = \{x_1, x_2, \dots, x_n\}$ . In a GP, any such set of random function follows a multivariate Gaussian distribution, which means that every linear combination of its components  $f = a_1x_1 + a_2x_2 + \dots + a_nx_n$  is normally distributed for any

vector  $\mathbf{a} \in \mathcal{R}^k$ . A Gaussian process follows a normal distribution and is therefore completely defined by its mean and covariance functions [25]:

$$f(x) \sim \mathcal{N}(m(x), K(x, x'))$$

with mean  $m(x)$  and covariance function  $K(x, x')$ . In this study, the mean function was fixed to zero ( $m(x) = 0$ ), which was not a strong limitation since the data can be centered in a pre-processing step. A squared exponential covariance was used as covariance function:

$$K(x, x') = \sigma_f^2 e^{-\frac{(x-x')^2}{2l^2}}$$

where  $l$  is the characteristic length-scale and  $\sigma_f^2$  controls the overall variance of the process.

In realistic modeling situations, only noisy data are available of the output function values. Therefore a Gaussian noise  $\varepsilon$  was added to the data such as:  $y = f(x) + \varepsilon$ , having a zero mean and a variance  $\sigma_n^2$ . The parameters  $l$ ,  $\sigma_f^2$  and  $\sigma_n^2$  correspond to the hyperparameter  $\theta$  characterizing the GP model. The hyperparameters that best represent all data in the training set are obtained by maximizing the Gaussian likelihood amongst the training dataset:

$$\log p(y|X, \theta) = -\frac{1}{2} y^T C^{-1} y - \frac{1}{2} \log |C| - \frac{n}{2} \log 2\pi$$

where  $C = K(x, x') + \sigma_n^2 I$  is the covariance function for the noisy targets  $y$ . The first term can be interpreted as a data-fit term, the second term is a complexity penalty and the last term is a normalizing constant.

#### 2.4.3 Gaussian Process Prediction

In order to make predictions, the Zernike coefficients estimated for the test dataset were compared with the stress-free shape resulting from the iterative process. The prediction  $y_{tp}^m$  of the  $m^{th}$  Zernike coefficient defined in the output of test dataset  $y_t$  is obtained as:

$$mean(y_{tp}^m) = K(x_t, x_s) [K(x_s, x_s) + \sigma_n^2 I]^{-1} y_s^m = K(x_t, x_s) \alpha_m$$

$$cov(y_{tp^m}) = K(x_t, x_t) - K(x_t, x_s)[K(x_s, x_s) + \sigma_n^2 I]^{-1}K(x_s, x_t)$$

where  $K$  is the covariance function,  $x_s$  and  $x_t$  are the training and the test input respectively, and  $y_s^m$  is the output of the training data. The first formula establishes that a linear predictor of the test output  $y_{tp^m}$  obtained by multiplication of the covariance between training and test input by a pre-computed vector  $\alpha_m$ , which only depends on training data.

Several optical parameters have been used to quantify the error of the GP predictions. These parameters included the keratometric indices, average curvature indices and wavefront aberration parameters. Keratometric indices are based on the average curvature of the steepest (SimKs) and flattest (SimKf) meridian on the corneal surface (given in diopters). They are calculated over a central corneal annulus of 0.5 to 2.5mm radius. The keratometric indices are the induced cylinder (SimKs – SimKf) and the induced change in average K (SimKs+SimKf)/2.0. Averaged axial curvature indices describe corneal shape in three important regions; the central, paracentral, and peripheral zones. Central average curvature is calculated over the central annulus of 0.0 to 2.0mm radius, the paracentral average curvature is calculated over an annulus of 2.0 to 3.5mm radius and the peripheral average curvature is calculated over an annulus of 3.5 to 5.0mm radius. Wavefront aberration is calculated from surfaces and is described by the following indices given as the average of the coefficients obtained by Zernike decomposition of the anterior cornea; the spherical aberration ( $Z_4^0$ ), coma ( $(Z_3^{-1} + Z_3^1)/2$ ), trefoil ( $(Z_3^{-3} + Z_3^3)/2$ ), tetrafoil ( $(Z_4^{-4} + Z_4^4)/2$ ) and the root mean square (RMS) of the aberrations of order 4 and higher ( $>Z_3^x$ ).

### 3 Results

The Gaussian process has been run to predict each Zernike coefficient required for the description of the anterior and posterior surfaces of every patients' stress-free shapes. The output of the GP includes the mean of the predicted variable as well as the variance associated with this parameter (Figure 2).

Four GP models have been created by gradually increasing the number of training data respectively 250, 500, 750, 1663. For a quantitative analysis, optical indices describing the stress-free shape have been considered. Differences calculated between the optical indices of the stress-free shape obtained with the pre-stressing iterative approach and the optical indices of the stress-free shape predicted with the GP model showed that for almost all optical indices, the curvature error did not exceed 0.025 D, while the wavefront aberration percentage error did not overcome 5%. This limit has been chosen because 0.025D is ten times smaller than an optical error perceptible by the patient. Moreover, results showed that the mean error was always around zero while the standard deviation of the error decreased with increasing size of the training data, reaching a plateau at about 1000 Training Data (Figure 3). Additionally, the corneal surface predicted using the GP model were analyzed. The Instantaneous Curvature maps of the stress-free shape, obtained with the pre-stressing iterative approach were compared to the maps obtained using the Zernike coefficients predicted by the Gaussian Model. The maps produced using the prediction model were qualitatively identical to the target corneal shape (Figure 4).

Two GP models were calculated to determine if separating healthy from pathological corneas in the training dataset could improve the predictions. For all the optical parameters, the mean error was always around zero. Results indicated that the training dataset including only healthy cornea provide slightly better predictions for healthy cornea than pathological ones. The opposite was also true; the pathological training dataset provide a better estimation of the stress-free shape of pathological corneas than of healthy ones (Table 1). However, the difference observed on the optical parameters remained small, which indicates that the model based on pathological training data is not able to significantly improve the predictions in pathological situations. In addition, with the model built on healthy corneas, 95% of the predictions remain within the boundaries of the targeted accuracy.

The predicted stress-free configurations were then used to calculate the shape of the cornea after physiological loading. The comparison of the stressed shape with the target topographic

measurements acquired on the patients, showed that the curvature mean error differs from zero in almost all cases, indeed most GP predictions lead to curvature errors exceeding the range of 0.025D (Table 2). In the worst case, the error could reach 0.05 D when the GP model was created by considering only pathological corneas. Besides, it seems that GP induced a slight underestimation of the central average curvature and a small overestimation of the peripheral average curvature in all cases. Overall, the results of the stressed shape showed that 80% of the patients had small prediction errors ( $<0.025D$  and  $<5\%$ ) on all the shape parameters simultaneously and 93% of the patients in the test group had all the shape parameters below the accuracy acceptable clinically ( $<0.05D$  and  $<10\%$ ).

## 4 Discussion

Recently, numerical models have also been proposed as tools to better understand the effect of surgeries on the eye, to support surgical intervention and to predict the refractive outcome [9, 10]. To reach these goals, mechanical properties of cornea and sclera have been characterized [11,12,13,14] and an accurate description of the shape of the patients' corneas has been provided by ophthalmological measurement devices. Since the measured shape is under tension due to the intra-ocular eye pressure, this information cannot be directly used to perform patient-specific simulation; hence a pre-stressing approach is necessary. Simulation time is always a critical point for clinical application. Therefore, the pre-stressing calculation phase represents a strong limitation to the dissemination of biomechanical planning to clinical applications. A non-parametric approach has been used to predict the stress-free configuration of the cornea in real time.

The results obtained with this method showed that the prediction accuracy could reach a level suitable for a clinical application. The current topographic devices used to measure the shape of the cornea reach an accuracy of  $\pm 0.25 D$ . In this work, we aimed at reaching an accuracy of 0.025 D for corneal shape stresses by the IOP, which is 10 times better than the accuracy of the input data. Results showed that for a GP model fitted on healthy data, the

target accuracy has been achieved for most of the optical parameters, but the prediction accuracy always remained below 0.05 D, which is 5 times better than the accuracy provided by the input devices. Considering that curvature information is challenging to predict, the level of accuracy reached with the proposed approach is high and seems appropriate for surgical planning. In all cases, accuracy of the predictions was largely superior to the precision of modern topography devices.

Different prediction models can be used according to the patient demographic information such as age, sex or specific pathology. In this study, a rough separation of the data has been performed between healthy and pathological. The results indicated that models solely based on pathological datasets were not able to better predict the stress-free configuration of the pathological data. A possible explanation is that many different ophthalmic diseases were combined inside this pathological group, but with a small number of instances for each of the pathologies. There are many different corneal changes induced by pathology; for example a keratoconus shows completely different corneal shapes than a Fuchs-Endothelial dystrophy. It is also clinically known that Laser-Assisted in situ Keratomileusis (LASIK) treated by tissue saving algorithms induces a spherical aberration. Due to the amount of patient information available, it was not possible to refine the analysis and propose disease-specific models, but we believe that such models would further improve the prediction accuracy.

Under physiological loading, the stress-free configuration should match the shape of the Pentacam data acquired on the patients. Our calculations indicate that the minor deviations observed on the stress-free configuration were amplified by the application of the internal ocular pressure. However, the results achieved with this method remain close to the target accuracy for 95% of the samples. In addition, all the optical parameters have a mean prediction very close to the experimental data, but the standard deviation of the prediction error increased during pre-stressing. Again, when the GP model is built on healthy data, results showed that the predictions are acceptable for clinical applications and that the

accuracy of the reconstructed shape remains at least five times better than the accuracy of current topographic tools.

The GP process proved to be an efficient technique to quickly predict the stress-free shape of the cornea. However, the method relies on a large database of pre-calculated results. This means that computational resources required to run the finite element simulations was not suppressed, but shifted in a pre-processing step. Despite the burden to run a large number of FE simulations, this approach has some benefits. The calculations are performed offline and can be verified by simulation experts avoiding any potential problem with model configuration, simulation convergence or other simulation errors. Dedicated hardware can be used for this purpose and the nature of the problem makes it easily parallelizable. As a consequence, a verified model can be delivered to the clinician. In addition, a relatively low number of input data was required to establish accurate prediction models. Results indicated that 1000 patient datasets were sufficient to reach a plateau in the prediction accuracy.

The proposed method relies on the Zernike coefficient for the prediction of the shape, which differs from the other pre-stressing approaches that rely on a finite element mesh. One of the benefits of the Zernike coefficient is that it is a direct representation of the refractive surface. The same approach based on finite element meshes would introduce inaccuracies from the discretization and from the mapping of the nodes on the surface. The establishment of correspondence on the corneal surface is difficult due to the lack of obvious landmarks. In addition, the Zernike coefficients enable an arbitrary meshing of the stress-free configuration, including eventual cut representing the surgical intervention.

The GP predictions proposed in this study are fitted to numerical simulations, which were performed with a precise set of material parameters, boundary conditions and loads. Although the finite element mesh selected doesn't affect the predictive model, alteration of any other parameter defining the finite element model implies rebuilding the complete model. This means that any improvement of the numerical model leads to heavy calculations since it requires re-establishing the database of pre-calculated results. This limitation is mitigated by



the facts that the process can be mostly automated, that a relatively small number of input models is required and that proper validation of the initial finite element model should be performed before building this database.

The application of the GP model has been limited to the prediction of the stress free shape of the cornea, because this corresponds to the most time consuming part of the overall planning procedure. However, the proposed technique can be extended to include more parameters representing the surgical intervention. Many refractive surgeries can be described with a small number of parameters describing the length, depth and position of the cut on the cornea. Of course, including the planning parameters in the predictive model is expected to significantly increase the size of the training data. On the other hand, such predictive model will provide the surgeon with real time prediction of the refractive outcome and opens the door to truly optimize the surgical parameters.

Ophthalmology is very demanding in terms of accuracy, where surface topology is measured in microns and curvature changes of a fraction of a diopter affect the patient's vision. In addition, existing tools are available to quantify the shape of the tissue as part of clinical routine, which enables the collection of a database of patient data to build and validate prediction models. For these reasons, ophthalmology represents an ideal application for new techniques aiming at predicting the stress shape of soft tissues. Based on the prediction accuracy obtained on the stress-free prediction of the cornea, we conclude that this technique is suitable as a first step of refractive planning solution. In addition, the same approach could be used to predict the internal stresses of other soft tissue such as arteries or ligaments.

## **5 Acknowledgements and declarations**

Elena Businaro and Harald Studer are employed by Integrated Scientific Services AG, a company developing "Optimeyes" a software to plan refractive surgeries. Bojan Pajic is a member of the Scientific Advisory Board of Optimeyes.

Philippe Buechler has no conflicts of interest to declare.

This research has been supported by the Swiss Innovation Promotion Agency through the grant number 13404.1 PFFLE-LS

Ethical approval was not required for this study.

## 6 References

[1] Gee, M.W., Förster, C., Wall, W.A., 2010. A computational strategy for prestressing patient-specific biomechanical problems under finite deformation. *International Journal for Numerical Methods in Biomedical Engineering* 26, (1):52–72.

[2] Grytz, R., Downs, J.C., 2012. A forward incremental prestressing method with application to inverse parameter estimations and eye-specific simulations of posterior scleral shells. *Computer Methods in Biomechanics and Biomedical Engineering*.

[3] Bols, J., Degroote, J., Trachet, B., Verheghe, B., Segers, P., Vierendeels, J., 2013. A computational method to assess the in vivo stresses and the unloaded configuration of patient-specific blood vessels. *Journal of Computational and Applied Mathematics* 246, 10-17.

[4] Hsu, M.-C., Bazilevs Y., 2011. Blood vessel tissue prestress modeling for vascular fluid–structure interaction simulation. *Finite Elements in Analysis and Design* 47, 593–599.

[5] Govindjee, S., Mihalic, P.A., 1998. Computational methods for inverse deformations in quasi-incompressible finite elasticity. *Journal for Numerical Methods in Biomedical Engineering* 43, (5):821–38.

[6] Govindjee, S., Mihalic, P.A., 1996. Computational methods for inverse finite elastostatics. *Computer Methods in Applied Mechanics and Engineering* 136, (1–2):47–57.

[7] Lu, J., Zhou, X., Raghavan, M.L., 2007. Inverse elastostatic stress analysis in pre-deformed biological structures: demonstration using abdominal aortic aneurysms. *Journal of Biomechanics* 40, (3):693–6

367 [8] Lanchares, E., Calvo, B., Cristóbal, J.A., Doblaré, M., 2008. Finite element simulation of  
368 arcuates for astigmatism correction. *Journal of Biomechanics* 41, (4):797–805.

369 [9] Pandolfi, A., Holzapfel, G.A., 2008. Three-dimensional modeling and computational  
370 analysis of the human cornea considering distributed collagen fibril orientations. *Journal of*  
371 *Biomechanical Engineering* 130, (6):061006.

372 [10] Roy, A.S., Dupps, W.J., 2011. Patient-specific modeling of corneal refractive surgery  
373 outcomes and inverse estimation of elastic property changes. *Journal of Biomechanical*  
374 *Engineering* 133, (1):011002.

375 [11] Pandolfi, A., Fotia, G., Manganiello, F., 2009. Finite element simulations of laser  
376 refractive corneal surgery. *Engineering with Computers* 25, 15–24.

377 [12] Elsheikh, A., Geraghty, B., Rama, P., Campanelli, M., Meek, K.M.,  
378 2010. Characterization of age-related variation in corneal biomechanical properties. *Journal*  
379 *of Royal Society Interface* 7, 1475–85.

380 [13] Elsheikh, A., Geraghty, B., Alhasso, D., Knappett, J., Campanelli, M., Rama, P.,  
381 2010. Regional variation in the biomechanical properties of the human sclera. *Experimental*  
382 *Eye Research* 90, 624–33.

383 [14] Elsheikh, A., Brown, M., Alhasso, D., Rama, P., Campanelli, M., Garway- Heath, D.,  
384 2008. Experimental assessment of corneal anisotropy. *Journal of Refractive Surgery* 24,  
385 (2):178–87.

386 [15] Yun, Y., Kim, H., Shin, S. Y., Lee, J., Deshpande, A. D., Kim, C., 2014. Statistical  
387 method for prediction of gait kinematics with Gaussian process regression. *Journal of*  
388 *Biomechanics* 47, 186-192.

389 [16] Ijaz, A., Choi, J., Lee, W., Baek, S., 2013. Prediction of Abdominal Aortic Aneurysms  
390 Using Sparse Gaussian Process Regression. *ASME Summer Bioengineering Conference*,  
391 *SBC 2013*. 2013; 1B.

- 392 [17] Dadashi, F., Millet, G.P., Aminiam, K., 2013. Gaussian process framework for pervasive  
393 estimation of swimming velocity with body-worn IMU. *Electronics Letters- IEE* 49(1). 44-46.
- 394 [18] Zernike, F., (1934). "Beugungstheorie des Schneidensverfahrens und Seiner  
395 Verbesserten Form, der Phasenkontrastmethode". *Physica* 1, (8): 689–704.
- 396 [19] Studer, H., Larrea, X., Riedwyl, H., Buchler, P., 2010. Biomechanical model of human  
397 cornea based on stromal microstructure. *Journal of Biomechanics* 43, 836–842.
- 398 [20] Studer, H. P., Riedwyl, H., Amstutz, C. A., Hanson, J. V. M., Buchler, P. 2013. Patient-  
399 specific finite-element simulation of the human cornea: A clinical validation study on cataract  
400 surgery. *Journal of Biomechanics* 46, 751–758.
- 401 [21] Markert, B., Ehlers, W., Karajan, N., 2005. A general poly convex strain-energy function  
402 for fiber-reinforced materials. *Proceedings in Applied Mathematics and Mechanics* 5, 245.
- 403 [22] Aghamohammadzadeh, H., Newton, R., Meek, K., 2004. X-ray scattering used to map  
404 the preferred collagen orientation in the human cornea and limbus. *Structure* 12, 249–256.
- 405 [23] Elsheikh, A., Wang, D., Brown, M., Rama, P., Campanelli, M., Pye, D., 2007.  
406 Assessment of corneal biomechanical properties and their variation with age. *Current Eye*  
407 *Research* 32, 11–19.
- 408 [24] Elsheikh, A., Whitford, C., Hamarashid, R., Kassem, W., Joda, A., Büchler, P., (2012).  
409 Stress free configuration of the human eye. *Medical Engineering and Physics* 35, 211– 216.
- 410 [25] Rasmussen, C.E., 2006. *Gaussian Processes for Machine Learning*.

412

413

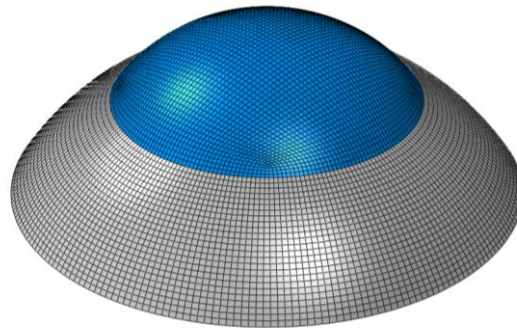


*Figure1: Spherical finite element mesh of the cornea, which was used as a template to mesh the patients' anatomy obtained in-vivo. The blue and the gray parts represent the cornea and the sclera respectively.*

414

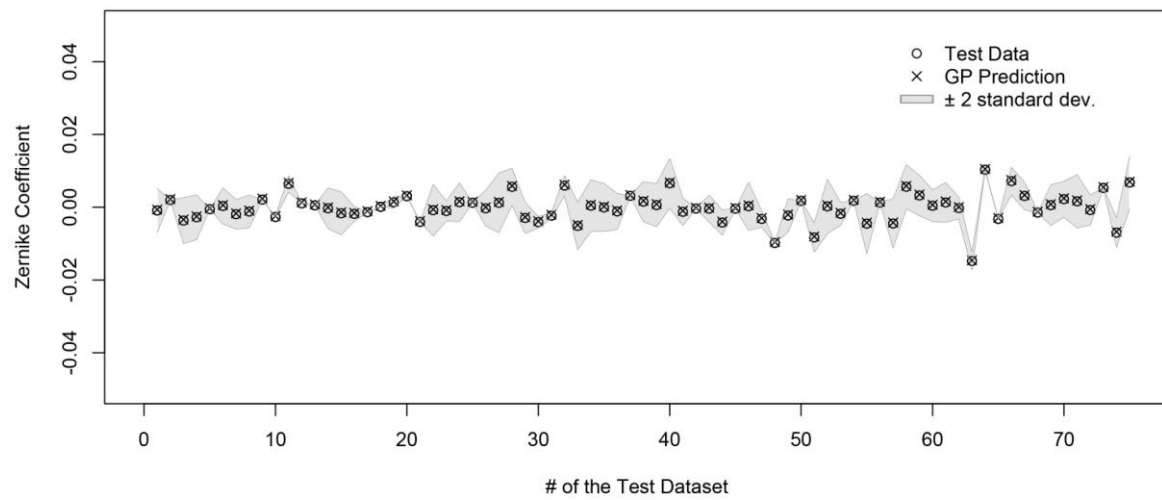


Figure 2: A Gaussian Model has been created with 250 Training Data. The graphs represent the results of prediction for one Zernike coefficient for each of the of 75 test data. The circles indicate the test data while the crosses are the GP prediction. The gray area representstwo standard deviationsas estimated by the GP predictions.

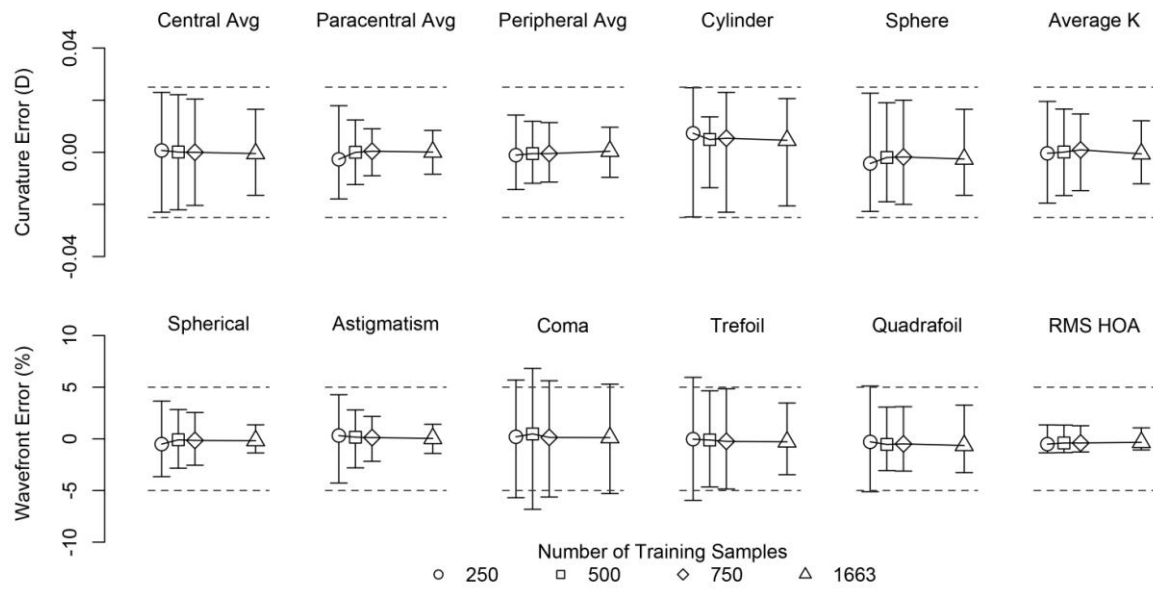


Figure 3: Accuracy of the GP prediction on the optical parameters of the cornea. The absolute mean error has been calculated in diopter (top) and the mean error on the wavefront aberration has been reported in percent (bottom). For each optical parameter, the accuracy of the prediction was reported for different size of the training data (250, 500, 750 and 1663). The error bars represented the variability of the data in a confidence interval of 95%. For most of the cases, the prediction error remains below the limits acceptable for clinical applications indicated by the dashed lines.

418

419

420

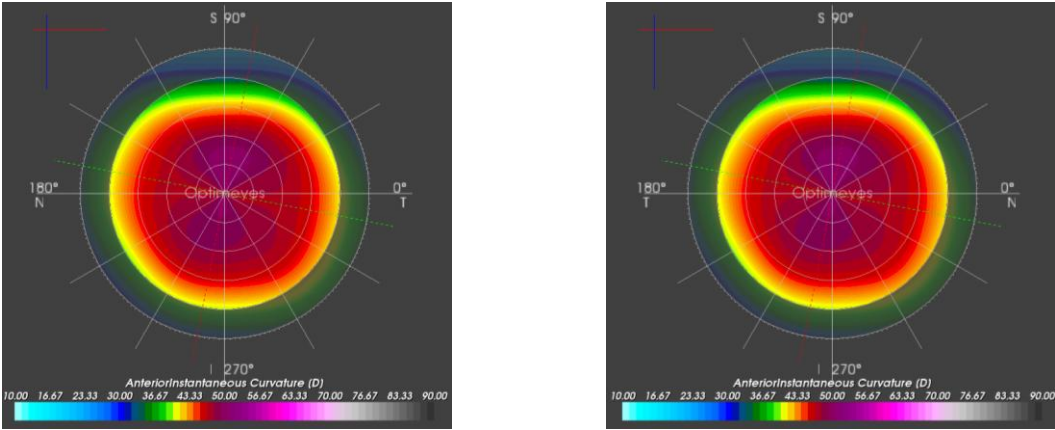


Figure 4: Instantaneous curvature obtained for the stress-free configuration obtained using the pre-stressing process (left) and predicted by the Gaussian model (right) for one of the reconstructed instance.

421



Stress Free Configuration		Healthy Training (700 datasets)		Pathological Training (700 datasets)	
		Healthy Test	Pathological Test	Healthy Test	Pathological Test
		(72 Dataset)	(71 datasets)	(72 Dataset)	(71 datasets)
Curvature (D)	Average K	-0.0008 ± 0.0136	0.0015 ± 0.0247	-0.0006 ± 0.0155	-0.0005 ± 0.0178
	Cylinder	0.0061 ± 0.0245	0.0091 ± 0.0294	0.0059 ± 0.0220	0.0057 ± 0.0165
	Central Avg	-0.0010 ± 0.0184	0.0038 ± 0.0399	-0.0007 ± 0.0194	0.0004 ± 0.0215
	ParacentralAvg	-0.0013 ± 0.0111	-0.0003 ± 0.0101	-0.0008 ± 0.0145	-0.0004 ± 0.0164
	Peripheral Avg	-0.0010 ± 0.0107	0.0008 ± 0.0100	-0.0024 ± 0.0200	-0.0001 ± 0.0145
Wavefront aberration (%)	Spherical	-0.21% ± 2.38%	-0.30% ± 3.53%	-0.11% ± 2.63%	-0.30% ± 1.79%
	Astigmatism	0.06% ± 2.26%	-0.07% ± 1.66%	0.17% ± 2.98%	0.10% ± 1.75%
	Coma	0.14% ± 6.26%	-0.47% ± 3.77%	0.25% ± 5.20%	-0.26% ± 3.63%
	Trefoil	-0.24% ± 4.34%	-0.07% ± 4.26%	0.03% ± 5.12%	-0.05% ± 5.28%
	Quadrafoil	-0.51% ± 3.54%	0.10% ± 7.76%	-0.49% ± 3.51%	0.20% ± 7.43%
	RMS HOA	-0.33% ± 1.09%	-0.21% ± 1.83%	-0.42% ± 1.17%	-0.32% ± 1.13%

Table1: Prediction error for the stress-free configurations calculated based on the GP. The error is indicated in diopters for the curvature parameters and in percent for the error on the wavefront aberration. The color code indicates the suitability of the predictions for clinical applications; green shows small prediction errors ( $<0.025D$  or  $<5\%$ ), yellow moderate prediction errors ( $0.025 - 0.05D$  or  $5 - 10\%$ ). The average values is shown as well the 95% confidence interval (i.e. two standard deviations).

		Healthy Training (700 datasets)		Pathological Training (700 datasets)	
Stressed Configuration		Healthy Test	Pathological Test	Healthy Test	Pathological Test
		(72 Dataset)	(71 datasets)	(72 Dataset)	(71 datasets)
Curvature (D)	Average K	-0.0065 ± 0.0129	-0.0039 ± 0.0253	-0.066 ± 0.0151	-0.0050 ± 0.0165
	Cylinder	0.0050 ± 0.0153	0.0092 ± 0.0400	0.0066 ± 0.0204	0.0099 ± 0.0433
	Central Avg	-0.0081 ± 0.0192	-0.0046 ± 0.0379	-0.0083 ± 0.0190	-0.0066 ± 0.0194
	ParacentralAvg	-0.0011 ± 0.0124	-0.0007 ± 0.0109	-0.0008 ± 0.0153	-0.0010 ± 0.0155
	Peripheral Avg	0.0139 ± 0.0132	0.0139 ± 0.0133	0.0128 ± 0.0169	0.0130 ± 0.0145
WavefrontAberratio	Spherical	0.73% ± 2.78%	0.55% ± 3.37%	0.86% ± 3.56%	0.53% ± 1.56%
	Astigmatism	0.04% ± 3.57%	0.15% ± 3.59%	0.08% ± 4.77%	0.20% ± 3.62%
	Coma	0.08% ± 4.66%	0.08% ± 3.26%	0.05% ± 7.17%	0.23% ± 2.67%
	Trefoil	-0.12% ± 4.36%	0.55% ± 5.19%	0.06% ± 3.89%	0.52% ± 4.39%
	Quadrafoil	0.19% ± 2.44%	-0.16% ± 2.67%	0.39% ± 2.76%	0.06% ± 2.67%
n (%)	RMS HOA	0.61% ± 0.86%	0.57% ± 1.41%	0.53% ± 0.92%	0.48% ± 0.89%

Table2: Prediction error for the stressed shape of the cornea obtained by simulating the internal ocular pressure on the stress-free configuration. The values reported in the table correspond to the difference between the prediction of the stressed shape using finite element simulation and the original topographic measurements. The error is indicated in diopters for the curvature parameters and in percent for the wavefront aberration errors. The color code indicates the suitability of the predictions for clinical applications; green shows small prediction errors (<0.025D or <5%), yellow moderate prediction errors (0.025 – 0.05D or 5 – 10%) and red shows prediction error that are considered as too large to ensure reliable surgical planning (>0.05D or >10%). For each parameter, the value represents the mean as well the 95% confidence interval (i.e. two standard deviations).

424

425